Remote Sensing of Environment 114 (2010) 2575–2583

Contents lists available at ScienceDirect

Remote Sensing of Environment

journal homepage: www.elsevier.com/locate/rse

Improved algorithm for MODIS satellite retrievals of aerosol optical thickness over land in dusty atmosphere: Implications for air quality monitoring in China

Jun Wang [a,b,*], Xiaoguang Xu [a], Robert Spurr [c], Yuxuang Wang [d], Easan Drury [e]

[a] Department of Earth and Atmospheric Sciences, University of Nebraska-Lincoln, Lincoln, NE, USA
[b] Code 613.2, Climate and Radiation Branch, NASA Goddard Space Flight, Greenbelt, MD, USA
[c] RT Solutions Inc., Cambridge, MA, USA
[d] Department of Environmental Science and Engineering, Tsinghua University, Beijing, China
[e] Strategic Energy Analysis Center, National Renewable Energy Lab, Golden, CO, USA

ARTICLE INFO

Article history:
Received 1 February 2010
Received in revised form 27 April 2010
Accepted 26 May 2010

Keywords:
Remote sensing of aerosols
Particulate matter air quality
Atmospheric correction in dusty condition
Air quality in China

ABSTRACT

A new algorithm, using the Moderate Resolution Imaging Spectroradiometer (MODIS) satellite reflectance and aerosol single scattering properties simulated from a chemistry transport model (GEOS-Chem), is developed to retrieve aerosol optical thickness (AOT) over land in China during the spring dust season. The algorithm first uses a "dynamic lower envelope" approach to sample the MODIS dark-pixel reflectance data in low AOT conditions, to derive the local surface visible (0.65 μm)/near infrared (NIR, 2.1 μm) reflectance ratio. Joint retrievals of AOT at 0.65 μm and surface reflectance at 2.1 μm are then performed, based on the time, location, and spectral-dependent single scattering properties of the dusty atmosphere as simulated by the GEOS-Chem. A linearized vector radiative transfer model (VLIDORT) that simultaneously computes the top-of-atmosphere reflectance and its Jacobian with respect to AOT, is used in the forward component of the inversion of MODIS reflectance to AOT. Comparison of retrieved AOT results in April and May of 2008 with AERONET observations shows a strong correlation ($R=0.83$), with small bias (0.01), and small RMSE (0.17); the figures are a substantial improvement over corresponding values obtained with the MODIS Collection 5 AOT algorithm for the same study region and time period. The small bias is partially due to the consideration of dust effect at 2.1 μm channel, without which the bias is −0.05. The surface PM_{10} (particulate matter with diameter less than 10 μm) concentrations derived using this improved AOT retrieval show better agreement with ground observations than those derived from GEOS-Chem simulations alone, or those inferred from the MODIS Collection 5 AOT. This study underscores the value of using satellite reflectance to improve the air quality modeling and monitoring.

1. Introduction

Atmospheric aerosol is a major concern for climate prediction and public health, but records of global aerosol distributions have only become available in the last decade from dedicated satellite observations such as MODIS (Remer et al., 2008) and the Multiangle Imaging SpectroRadiometer (MISR) (Kahn et al., 2005). Despite much progress made recently in using satellite data to derive surface aerosol concentration over land (see Hoff and Christopher (2009) for a review), several challenges exist. The radiance or reflectance data collected by currently operational passive remote sensing instruments for aerosol retrieval are mostly at the atmospheric window channels in the visible spectrum. Therefore, they offer little information on aerosol vertical distribution beyond the retrieval of columnar properties such as aerosol optical thickness (AOT) (Wang et al., 2003a). In the near UV spectrum, the slope of the reflectance is regulated by height-dependent Rayleigh scattering and aerosol absorption, and this relationship can be used to estimate the centroid height of absorbing aerosols (Torres et al., 2007). However, such an algorithm requires *a priori* information on aerosol single scattering albedo to infer AOT, and it lacks sensitivity to changes in lower tropospheric aerosol mass. In contrast, active satellite remote sensing techniques such as the Cloud-Aerosol Lidar with Orthogonal Polarization (CALIOP) can provide vertical profiles of aerosol extinction, but when compared to the aerosol plume height retrieved from MISR, their daily observation offer very limited converge over the globe because of narrow sensor ground track (~100 m) (Kahn et al., 2008).

With very few observational constraints on aerosol vertical distribution, studies to date have had to use chemistry transport models (CTMs) to interpret the 2D satellite information of either AOT or reflectance into the 3D aerosol fields (Wang & Christopher, 2003; Al-Saadi et al., 2005). A common practice so far has been that the simulated aerosol mass at each vertical layer in a model grid box is updated by a scale factor that is the ratio of spatiotemporally -collocated AOT values from the model and the satellite retrieval algorithm (Wang et al., 2004; Liu et al., 2007; van Donkelaar et al., 2010). Resultant surface aerosol

* Corresponding author. Department of Earth and Atmospheric Sciences, University of Nebraska-Lincoln, 303 Bessey Hall, Lincoln, NE, 68588, USA. Tel.: +1 402 472 3597; fax: +1 402 472 4917.
E-mail address: jwang7@unl.edu (J. Wang).

0034-4257/$ – see front matter © 2010 Elsevier Inc. All rights reserved.
doi:10.1016/j.rse.2010.05.034

concentrations generally show better agreement with ground-based counterparts than those obtained without applying the scale factor, highlighting the value of the satellite AOT for the remote sensing of air quality (Hoff and Christopher, 2009).

Though simple in concept, the above approach has one "inconvenient truth". The set of aerosol single scattering properties used in the CTM to compute the AOT is inconsistent with the corresponding set employed in the satellite retrieval algorithm. This inconsistency not only adds difficulty and confusion to resolving discrepancies between modeled and satellite-retrieved AOT, but also makes CTM simulations constrained by the satellite-based aerosol products unable to reproduce reflectance data that the satellites actually measure. To overcome these issues, recent studies have started using satellite reflectance data to constrain the CTM simulations. The principle here is that aerosol mass fields in a CTM are iteratively updated (retrieved) until the reflectance computed from the CTM agrees with the satellite-measured reflectance, while the single scattering properties of each aerosol species are kept as generic (constant) if not explicitly simulated in the CTM (Drury et al., 2008; Weaver et al., 2007).

However, computations of top-of-atmosphere (TOA) reflectance require the input of the *surface* reflectance in addition to the CTM-simulated aerosol microphysics. For visibly dark surfaces such as heavily vegetated area, surface reflectance at 0.65 μm ($\rho_{0.65}^{SFC}$) can be approximated from the reflectance at 2.1 μm ($\rho_{2.1}^{SFC}$) with the relationship $\rho_{0.65}^{SFC} = \xi \rho_{2.1}^{SFC}$, where ξ primarily varies with phenology, canopy type, soil type and wetness at the surface but generally centers ~0.55 (Levy et al., 2007). This relationship has been used in Weaver et al. (2007) and Drury et al. (2008) to derive $\rho_{0.65}^{SFC}$ from the TOA reflectance at 2.1 μm (hereafter $\rho_{2.1}^{MDTOA}$), assuming that the atmosphere is transparent at 2.1 μm. Such assumption $\rho_{2.1}^{SFC} = \rho_{2.1}^{MDTOA}$ may be valid in conditions dominated by fine-mode aerosol. However, it is not true for dusty conditions, where large particles (with Angstrom exponent close to zero) can produce considerable extinction at 2.1 μm. In this case, an atmospheric correction is needed for $\rho_{2.1}^{MDTOA}$ before using it to estimate $\rho_{0.65}^{SFC}$.

In this paper, we develop an algorithm using MODIS reflectances and CTM simulations to perform AOT retrieval in dusty atmosphere. This study refines the method described in Drury et al. (2008) that demonstrated improved retrieval of AOT from MODIS over the U.S.A. in non-dusty conditions, and here we develop a new approach to minimize the retrieval uncertainties in dusty conditions for which atmosphere is not transparent at 2.1 μm. We apply our approach over the China during the spring dust season. We further demonstrate the utility of this improved retrieval method for air quality monitoring in China, by comparing our results with the operational MODIS AOT product and other *in situ* data.

2. Data sources and atmospheric models

We use the MODIS Level 2 Collection 5 aerosol product (Levy et al., 2007) at 10×10 km^2 (nadir) resolution from the Terra and Aqua satellites over the continental China during April and May 2008. The data consists of cloud-screened TOA reflectance at 0.65 μm and 2.1 μm over dark surface pixels (hereafter $\rho_{0.65}^{MDTOA}$ and $\rho_{2.1}^{MDTOA}$, respectively), and the corresponding AOT retrieved from the MODIS Collection 5 operational algorithm (hereafter $\tau_{0.65}^{MDC5}$). Other observations we used include the AOT data (level 2) collected by AErosol RObotic NETwork (AERONET) stations in China (Holben et al., 1998), and the daily-averaged concentration of PM_{10} (particulate matter with diameter less than 10 μm) collected by the Chinese EPA observation network at ~80 major cities (http://datacenter.mep.gov.cn/).

We simulate the 3D aerosol fields for the study time and location using a nested-grid version (v8.1.1) of the GEOS-Chem CTM (Chen et al., 2009; Fairlie et al., 2007; Park et al., 2004), driven by the NASA Goddard Earth Observing System (GEOS-5) assimilated meteorological fields at $0.5° \times 0.667°$ resolution. Detailed descriptions of the GEOS-Chem aerosol emission inventories and simulation evaluations are provided in Park et al. (2004) and Wang et al. (2008) for sulfur and ammonia, in Fairlie et al. (2007) for dust, and in Chen et al. (2009) for biomass burning aerosols and recent updates of emission inventories over the China region. The single scattering properties for each aerosol species (including dust, sulfate, nitrate, organic and black carbon aerosols) in GEOS-Chem are taken from Koepke et al. (1997), except that the geometric standard deviation for all non-dust aerosols are set to 1.6 (instead of 2.0) (Drury et al., 2010). An external mixture is assumed to sum over aerosol types to generate the AOT, the ensemble single scattering albedo, and the ensemble scattering phase function at each vertical model layer (Drury et al., 2008). All model outputs are saved at 3-hour intervals and interpolated to the satellite overpass time.

A linearized vector discrete ordinate radiative transfer (VLIDORT) model (Spurr, 2008) is used to compute the TOA reflectance and the Jacobian of this reflectance with respect to AOT for a given atmospheric column defined by the following inputs: (1) molecular (Rayleigh) and aerosol optical thickness, ensemble single scattering albedo, and ensemble phase functions at each vertical model layer, (2) spectral response functions of the MODIS instrument, (3) Sun–Earth–satellite geometry, and (4) surface reflectance estimated using the procedure described in Section 3.

3. Retrieval algorithm

The retrieval algorithm is an improvement over the study by Drury et al. (2008), and its flow chart is shown in Fig. 1. In low visible-AOT conditions where $\rho_{2.1}^{SFC} = \rho_{2.1}^{MDTOA}$ can be assumed, Drury et al. (2008) showed that the cloud-free $\rho_{0.65}^{MDTOA}$ (after scaling into the nadir) can be simplified into two terms:

$$\rho_{0.65}^{MDTOA}\,\mu_0\,\mu = \rho_{0.65}^{ATM} + \xi\,\rho_{2.1}^{MDTOA}\mu_0\,\mu\,T_{0.65}(\mu_0)\,T_{0.65}(\mu) \quad (1)$$

where the first term on the right is the atmospheric contribution due to Rayleigh and aerosol scattering, and the second term on the right is the surface contribution. $T_{0.65}(\mu_0)$ and $T_{0.65}(\mu)$ are respectively the downward and upward atmospheric transmission functions for the cosine of solar zenith angle, μ_0, and the cosine of satellite viewing zenith angle, μ. The Eq. (1) suggests that a linear regression for the lower envelope of $\rho_{0.65}^{MDTOA}\mu_0\mu$ and $\rho_{2.1}^{MDTOA}\mu_0\mu T_{0.65}(\mu_0)T_{0.65}(\mu)$ data pairs can be performed to derive ξ (the regression slope). In practice, we approximate T based upon the Rayleigh optical thickness (Drury et al., 2008), and we create a sample of lower envelope data pairs for each day and each GEOS-Chem grid box by gathering MODIS reflectance data over the 40-day period centered on that day over the same grid box. As shown in Section 4.2, we varied the length of this period used to derive ξ, and found that the 40 days was the optimal time interval. To ensure smoothness and to capture gradual changes of ξ due to the evolution of surface greenness over the two-month study period, we take a 5-day running average of the time series of ξ before application in the retrieval algorithm. We call the above procedure for deriving ξ the "dynamic lower envelope" approach, as opposed to the "static lower envelope" approach in Drury et al. (2008) where ξ was kept constant with time.

The computation of TOA reflectance at 0.65 μm based upon GEOS-chem simulated aerosol fields (hereafter $\rho_{0.65}^{GCTOA}$) starts with the estimate of $\rho_{2.1}^{SFC}$ from $\rho_{2.1}^{MDTOA}$, so that $\rho_{0.65}^{SFC}$ can be derived ($=\xi\rho_{2.1}^{SFC}$) as an input for VLIDORT (Fig. 1). The initial estimate of $\rho_{2.1}^{SFC}$ is made by using GEOS-Chem simulations of the timing and location of dust events to conduct a first-order single scattering correction of $\rho_{2.1}^{MDTOA}$:

$$\rho_{2.1}^{SFC} = \rho_{2.1}^{MDTOA} - \omega_{2.1}^{GC} P_{2.1}^{GC}(\Theta)\frac{1}{4(\mu+\mu_0)}\left[1 - e^{-\tau_{2.1}^{GC}\left(\frac{1}{\mu}+\frac{1}{\mu_0}\right)}\right] \quad (2)$$

where $\tau_{2.1}^{GC}$, $\omega_{2.1}^{GC}$ and $P_{2.1}^{GC}$ are the GEOS-Chem simulated AOT, aerosol single scattering albedo and phase function respectively at 2.1 μm; Θ

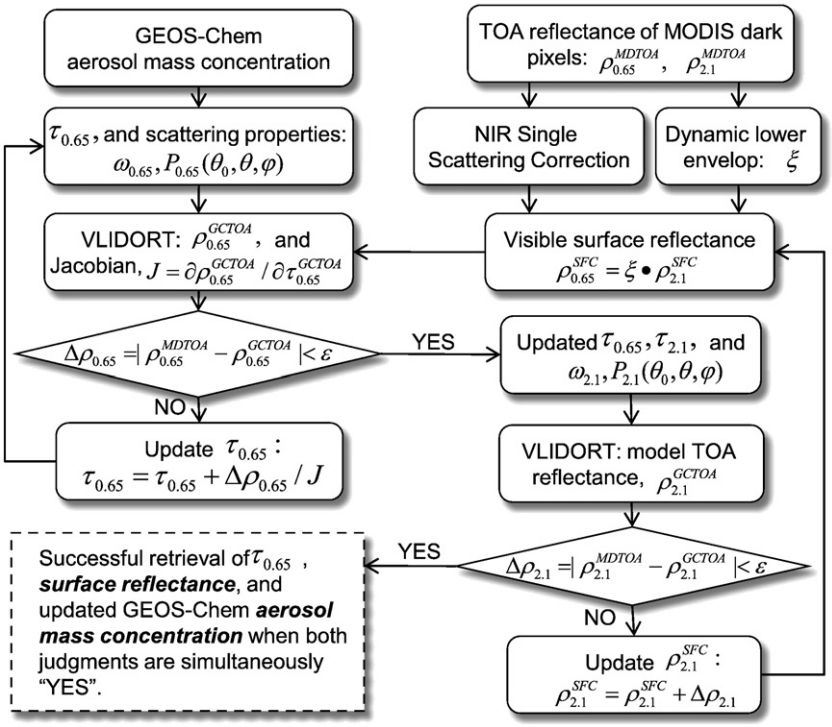

Fig. 1. The flow chart of the retrieval algorithm. See Section 3 in the text for detailed description.

is the scattering angle between the incident sun light and the reflected light viewed by the satellite. To account for the differences in the spatial resolution between GEOS-Chem and MODIS data, we followed Drury et al. (2008); at each grid box and each day, the GEOS-Chem simulated aerosol single scattering properties are interpolated to the satellite overpass time and then applied in the retrieval to all the MODIS pixels in that grid box. This is appropriate because the GEOS-Chem's spatial resolution is $0.5°\times0.67°$ which is sufficiently fine to capture typical spatial scale (40–400 km) for the variation of aerosol optical properties (Anderson et al., 2003).

From the above first guess of $\rho_{2.1}^{SFC}$, the retrieval steps are as follows (Fig. 1):

(1) Initialize the retrieved AOTs at 0.65 μm and 2.1 μm (hereafter $\tau_{0.65}^{MDGC}$ and $\tau_{2.1}^{MDGC}$, MDGC denotes MODIS plus GEOS-Chem) to the CTM values, $\tau_{0.65}^{GC}$ and $\tau_{2.1}^{GC}$.
(2) Compute $\rho_{0.65}^{GCTOA}$ and its Jacobian with respect to AOT ($\partial\rho_{0.65}^{GCTOA}/\partial\tau_{0.65}^{MDGC}$) using VLIDORT with inputs of $\rho_{0.65}^{SFC}$ ($=\xi\rho_{2.1}^{SFC}$), $\tau_{0.65}^{MDGC}$, and the CTM ensemble aerosol scattering properties at 0.65 μm.
(3) If $|\rho_{0.65}^{GCTOA}-\rho_{0.65}^{MDTOA}|$ is less than 0.001, go to step (5). Otherwise, update the retrieved AOT: $\tau_{0.65}^{MDGC}=\tau_{0.65}^{MDGC}+(\rho_{0.65}^{MDTOA}-\rho_{0.65}^{GCTOA})\,\partial\tau_{0.65}^{MDGC}/\partial\rho_{0.65}^{GCTOA}$.
(4) Repeat (2) and (3) until $|\rho_{0.65}^{GCTOA}-\rho_{0.65}^{MDTOA}|$ is less than 0.001; the end of this step essentially ensures the radiative closure at 0.65 μm.
(5) Scale the mass of aerosol species at each layer by a factor of $\tau_{0.65}^{MDGC}/\tau_{0.65}^{GC}$ to re-compute $\tau_{2.1}^{MDGC}$, and then calculate the TOA reflectance at 2.1 μm (hereafter $\rho_{2.1}^{GCTOA}$) using VLIDORT with inputs of $\tau_{2.1}^{MDGC}$, $\rho_{2.1}^{SFC}$, and GEOS-Chem aerosol scattering properties at 2.1 μm.
(6) If $|\rho_{2.1}^{GCTOA}-\rho_{2.1}^{MDTOA}|$ is less than 0.001, the retrieval is successful and the algorithm stops. Otherwise, update $\rho_{2.1}^{SFC}=\rho_{2.1}^{SFC}+\rho_{2.1}^{MDTOA}-\rho_{2.1}^{GCTOA}$.
(7) Repeat steps (1) to (6) until the pair of $\rho_{2.1}^{SFC}$ and $\tau_{0.65}^{MDGC}$ values is found such that $\rho_{2.1}^{GCTOA}$ and $\rho_{0.65}^{GCTOA}$ both have less than 0.001 (absolute) difference with $\rho_{2.1}^{MDTOA}$ and $\rho_{0.65}^{MDTOA}$, respectively. The threshold of 0.001 follows that of Drury et al. (2008).

The above retrieval approach is iterative, in contrast to the traditional look-up table approach (Levy et al., 2007). The iterations are guided by the VLIDORT output of Jacobian of reflectance with respect to AOT. Although the relationship between AOT and reflectance is non-linear, it can be regarded as piecewise linear. In this case, the VLIDORT-calculated Jacobian of reflectance with respect to AOT (such as $\partial\rho_{0.65}^{GCTOA}/\partial\tau_{0.65}^{MDGC}$) provides the relative direction (an increase or decrease) and magnitude needed for the adjustment of retrieved AOT in each iteration (step 4) so that the modeled reflectance rapidly approaches to the satellite-measured reflectance.

4. Results and discussion

4.1. Results

Regressions used for the deriving ξ in the "dynamic lower envelope" approach are found to be statistically significant at all times, with correlation coefficient generally larger than 0.95. The temporal variation of ξ in the same grid box over the two-month study period is generally less than ±5%. An example is shown in Fig. 2a for one of the AERONET stations in China (Xinglong), where the regression for ξ on April 1 explains 99% of data variability in the lower envelope of the visible vs. NIR reflectance scatter plot (the inset of Fig. 2a), and ξ changes from 0.55 in early April to around 0.64 at the end of May. As with surface phenology, such changes of ξ through time are not monochromatic (Fig. 2a); this is consistent with the findings of Levy et al. (2007), who showed that ξ generally increases with greenness (or vegetation index). The map of derived ξ averaged over two months (Fig. 2b) shows larger ξ (>0.55) in heavily vegetated or cultivated regions in the east, and smaller values for grasslands and semi-arid regions in the west; again, this is consistent with results in Levy et al. (2007) and Drury et al. (2008). Unexpectedly large ξ values (close to 0.8) associated with less statistically significant regression are found in a few GEOS-Chem grid boxes that contain water bodies (coastline, lakes, and seasonal agriculture irrigation in the southeastern China) or steep topography around the Sichuan basin (30°N, 105°E); this is consistent with Kaufman et al. (2002).

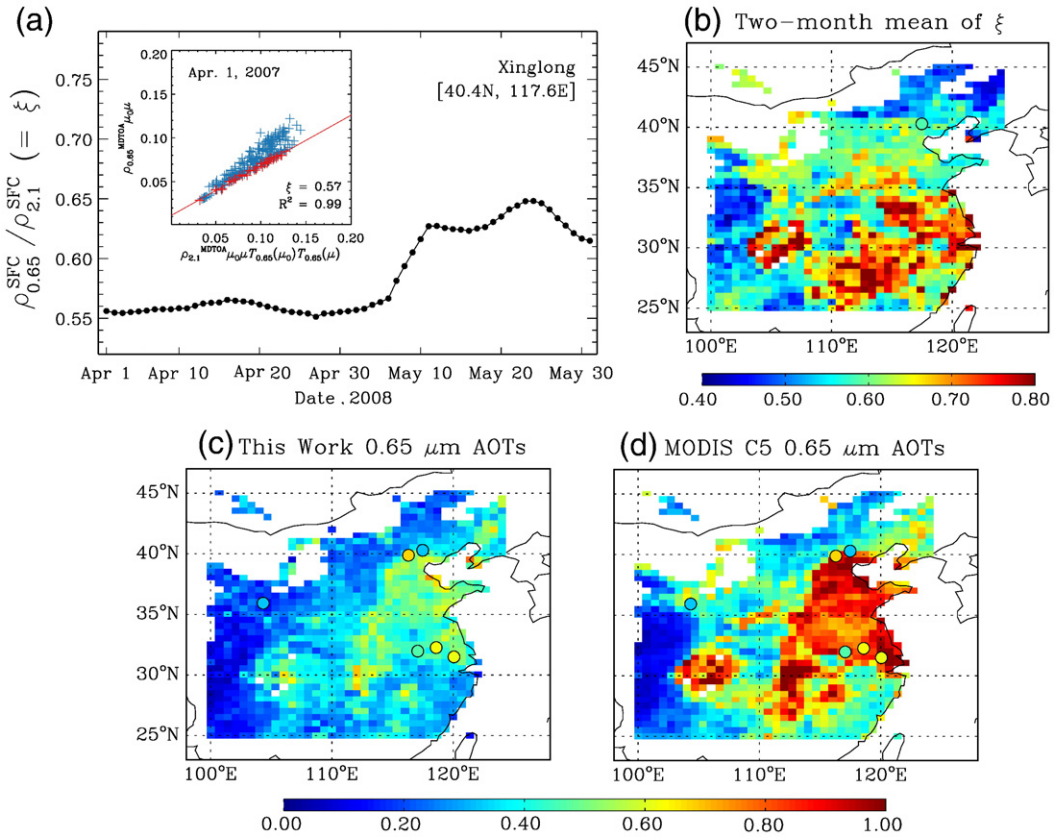

Fig. 2. (a) Time series of the derived ratio (ξ) between surface visible reflectance ($\rho^{SFC}_{0.65}$) and near infrared reflectance ($\rho^{SFC}_{2.1}$) for a GEOS-Chem grid box where an AERONET station, Xinglong, is located (the black circle in (b)). The inset shows the scatter plot of scaled top-of-atmosphere reflectances at 0.65 μm ($\rho^{MDTOA}_{0.65}\mu_0\mu$) and at 2.13 μm ($\rho^{MDTOA}_{2.1}\mu_0\mu T_{0.65}(\mu_0)T_{0.65}(\mu)$) collected by MODIS over a 40-day period centered on 1 April 2008, for that GEOS-Chem grid box. The red pluses identify the subset of reflectance data that constitutes the lower envelope of pairs used in the regression to find the slope ξ (see text for details). (b) Map of averaged ξ in April–May 2008 for each GEOS-Chem grid box in the area of this study. (c) and (d) respectively show maps of averaged AOTs (in April–May 2008) at 0.65 μm retrieved by this study and by the MODIS Collect 5 algorithm. The corresponding 2-month averages of AOT at 0.67 μm collected at 6 AERONET stations are color-coded as circles in (c) and (d).

The map of 2-month averages of $\tau^{MDGC}_{0.65}$ shows larger AOT values in densely-populated coastal regions and in the central industrialized area in China (Fig. 2c). Although the spatial distribution is similar to that of $\tau^{MDC5}_{0.65}$, $\tau^{MDGC}_{0.65}$ retrieved in this study is quantitatively smaller than $\tau^{MDC5}_{0.65}$ (Fig. 2d). In comparison with averages of AOT at 6 AERONET stations in China (color circles in Fig. 2c–d), $\tau^{MDC5}_{0.65}$ values clearly show a large positive bias, while virtually no systematic bias exists for $\tau^{MDGC}_{0.65}$.

To evaluate $\tau^{MDGC}_{0.65}$, spatially-averaged values of this quantity over a 50×50-km^2 area centered at an AERONET station is compared against temporally-averaged AOT measured at that station ($\tau^{AERT}_{0.67}$) within 30 min of the satellite overpass time (Ichoku et al., 2002). In total, 37 pairs of $\tau^{MDGC}_{0.65}$ and $\tau^{AERT}_{0.67}$ were found during the 2-month time period. As shown in Fig. 3a–b, the correlation coefficient (R) between $\tau^{MDGC}_{0.65}$and $\tau^{AERT}_{0.67}$ is 0.83, which is similar to its counterpart between $\tau^{MDC5}_{0.65}$and $\tau^{AERT}_{0.67}$($R=0.81$). However, regarding $\tau^{AERT}_{0.67}$ as ground truth, the bias (0.01) and RMSE (0.17) for $\tau^{MDGC}_{0.67}$ are both significantly smaller than their respective counterparts (0.12 and 0.23) for $\tau^{MDC5}_{0.65}$, quantifying the improvement in our AOT retrieval algorithm.

To analyze potential sources of retrieval error, the comparison data pairs in Fig. 3a–b are plotted using a color-coding based upon the corresponding $\tau^{GC}_{2.1}$ simulated from GEOS-chem. Interestingly, significant overestimations (>0.2 in average) in $\tau^{MDC5}_{0.65}$ appear to occur almost exclusively during the heavy dust conditions with $\tau^{GC}_{2.1}>0.2$, suggesting two possible error sources in the MODIS C5 aerosol retrieval algorithm: (a) $\rho^{SFC}_{0.65}$ is low, and (b) the single scattering albedo of coarse-mode aerosols (0.95 at 0.65 μm) is low. Given that aerosol scattering properties in the MODIS C5 algorithm are based upon a climatology derived from AERONET retrievals, the possibility (a) is more likely. This conjecture is supported by the fact that negative AOT retrievals (up to −0.05) are allowed in MODIS C5 algorithm, suggesting its need to improve the characterization of surface reflectance. In contrast, while $\tau^{MDGC}_{0.65}$ show a much lower positive bias during dusty conditions, it has a small negative bias (−0.07 in average) in non-dusty conditions. Sensitivity analysis of other retrieval error sources such as dust non-sphericity and single scattering albedo is our next-step research (see discussion in Section 4.2).

To check further the robustness of the above validation statistics, we also compared the time averages of retrieved AOTs with AERONET observations (Fig. 3c–d). Statistics were computed as a function of the number of days used in the average, for AOTs from three retrievals: $\tau^{MDC5}_{0.65}$, $\tau^{MDGC}_{0.65}$, and $\tau^{MDGC}_{0.65}$ without applying the atmospheric correction in 2.1 μm for deriving $\rho^{SFC}_{2.1}$ (hereafter $\tau^{MDGC}_{0.65,noAC}$). Overall, for a given number of days used in the average, RMSEs of $\tau^{MDGC}_{0.65,noAC}$ and $\tau^{MDGC}_{0.65}$are nearly equal; but both are considerably smaller than that of $\tau^{MDC5}_{0.65}$ (Fig. 3c). Furthermore, the decreasing trend of RMSE with time (from 1 to 9 days) is much larger for $\tau^{MDGC}_{0.65}$ (0.17 to 0.06) than that of $\tau^{MDC5}_{0.65}$ (0.23 to 0.15). In contrast, the biases in all three retrievals show little change with time, indicating that they are systematic. A large positive bias (0.12) is evident in $\tau^{MDC5}_{0.65}$, in comparison with biases of 0.01 in $\tau^{MDGC}_{0.65}$ and −0.05 in $\tau^{MDGC}_{0.65,noAC}$. In addition, the improved quality of $\tau^{MDGC}_{0.65}$ also shows up in the regression statistics (Fig. 3d): (a) the slope of the regression line (1.4–1.5) for $\tau^{MDC5}_{0.65}$ (with respect to $\tau^{AERT}_{0.67}$) shows a larger deviation from unity than that for $\tau^{MDGC}_{0.65,noAC}$ and $\tau^{MDGC}_{0.65}$ (both around 1.1–1.2), regardless of the averaging time; (b) when the

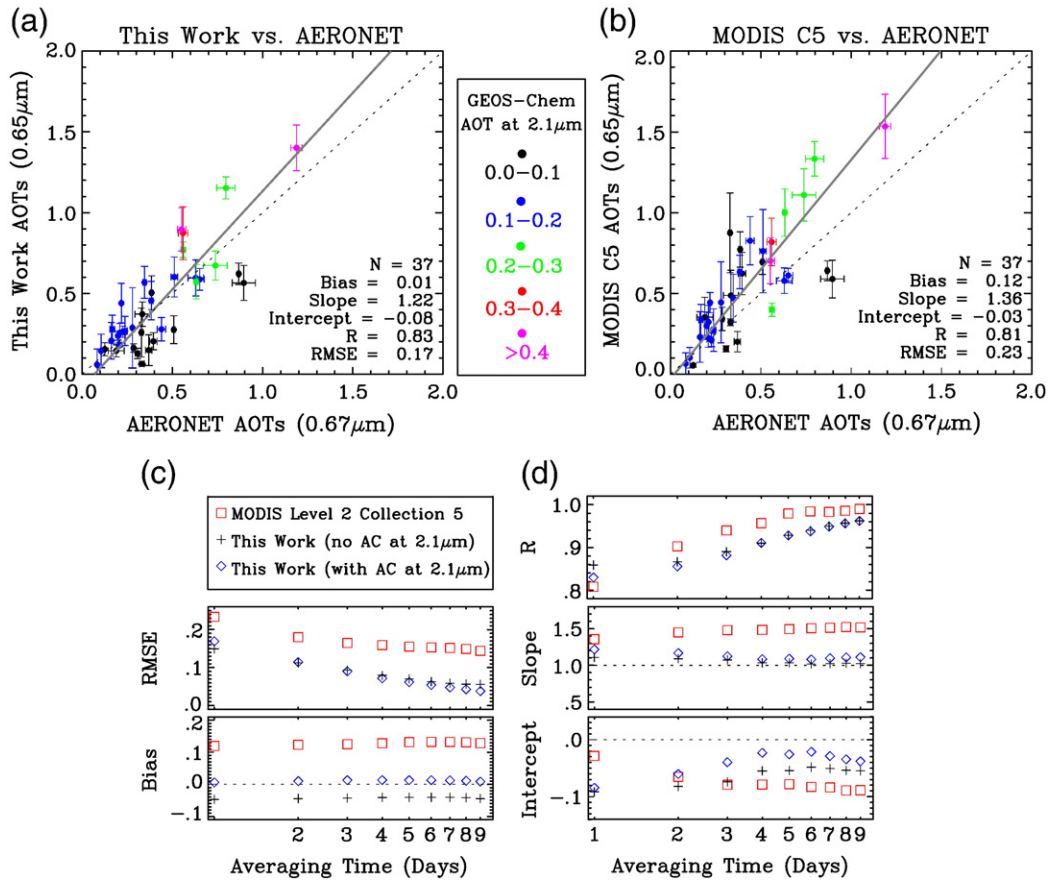

Fig. 3. (a) and (b) respectively show the comparison of spatiotemporally-collocated AOTs at 0.65 μm retrieved in this work and from MODIS Collection 5 with corresponding values from AERONET; symbols are color-coded based upon the AOT at 2.1 μm simulated by GEOS-chem (see text for details). Also shown are comparison statistics for a total number of data comparison pairs (N): mean bias, root mean square error (RMSE), correlation coefficient (R), and the slope and intercept of the linear regression line (in solid black). The one-to-one fit line is shown in dotted black. (c) and (d) show the statistics of comparison of AOTs from AEROENT with those retrieved by different algorithms for various averaging times from 1 to 9 days. Results from our algorithm with and without the atmospheric correction (AC) at 2.1 μm are plotted as black plus symbols and blue diamond symbols respectively, as opposed to the MODIS Collection 5 values (red squares). The comparison statistics include RMSE, bias, R, the slope, and the intercept of the linear regression line.

averaging time increases, the intercepts for both $\tau_{0.65,noAC}^{MDGC}$ and $\tau_{0.65}^{MDGC}$ decrease from −0.1 to −0.04, and thus move closer to zero than that for $\tau_{0.65}^{MDC5}$ (increases from −0.02 to −0.1). The R values for a given averaging time for $\tau_{0.65}^{MDC5}$ are either equivalent to or slightly better than those for $\tau_{0.65}^{MDGC}$, likely reflecting the co-variation of the systematic positive AOT bias with $\tau_{0.65}^{MDC5}$. Overall, the statistics of comparing time averages supports the finding in the instantaneous comparison, indicating a better agreement of $\tau_{0.65}^{MDGC}$ (than $\tau_{0.65}^{MDC5}$) with $\tau_{0.67}^{AERT}$.

The implication of improved AOT retrieval for the estimate of surface particulate matter concentration was studied by comparing PM_{10} data collected by the Chinese EPA at 62 cities in the study domain with those estimated from three different methods based upon: (i) GEOS-Chem simulation only (hereafter PM^{GC}), (ii) GEOS-Chem simulation scaled by $\tau_{0.65}^{MDC5}/\tau_{0.65}^{GC}$ (hereafter PM^{MDC5}), and (iii) GEOS-Chem simulations constrained by MODIS reflectance (i.e., scaled by $\tau_{0.65}^{MDGC}/\tau_{0.65}^{GC}$, hereafter PM^{MDGC}). While many cities in China have more than one site to routinely measure PM_{10} mass concentration, only the 24-h mean PM_{10} air quality index averaged over each city is available to this study. We convert the index to the PM_{10} mass concentration based upon the Chinese national ambient air quality standards, admitting that the large yet hard-to-be quantified errors can occur in using this dataset to represent the daily mean PM_{10} in each city (hereafter PM^{CEPA}). Hence, only the comparison of 2-month averages for each city is conducted here. Geographically (Fig. 4a–c), PM^{MDGC}clearly shows a better agreement than $PM^{MDC5}$and PM^{GC} with PM^{CEPA} in China at 33°N–45°N zone where most dust particles from Gobi and Taklamakan deserts are transported. Quantitatively (Fig. 3d–f), PM^{MDGC}, PM^{MDC5}, and PM^{CEPA} are found to have similar correlations with the PM^{CEPA}, but PM^{MDGC} shows smaller negative bias (−0.5 μg m^{-3}) and RMSE (46.6 μg m^{-3}) than PM^{MDC5} (bias 56.7, RMSE 86.7), and PM^{GC} (bias −37.5, RMSE 53.1). The large negative bias in GEOS-Chem simulation (presumably due to the uncertainty in emissions used in the model) is largely compensated when using the constraint of MODIS reflectance.

4.2. Discussion

In the results above, the derivation of the surface visible/near infrared reflectance ratio for a particular day uses the MODIS data over the 40-day period centered on that day. We have used MODIS data compilations for various values of the time window length (hereafter L) in our "dynamical envelope approach", and we found that a 40-day time period is optimal to meet the following two criteria. First, L should be long enough so that sufficient low-aerosol scenarios are present to ensure that the linear regression for deriving ξ is statistically significant. Second, L should be short enough and should center on the day for which ξ is to be derived in order that the temporal variation of ξ from the daily derivation can capture the gradual change of surface greenness. The derived value of ξ will not be temporally representative and indeed will have a time lag (or advance) to describe the evolution of surface phenological evolution if we use only the MODIS data before (or after) the day for which ξ is derived.

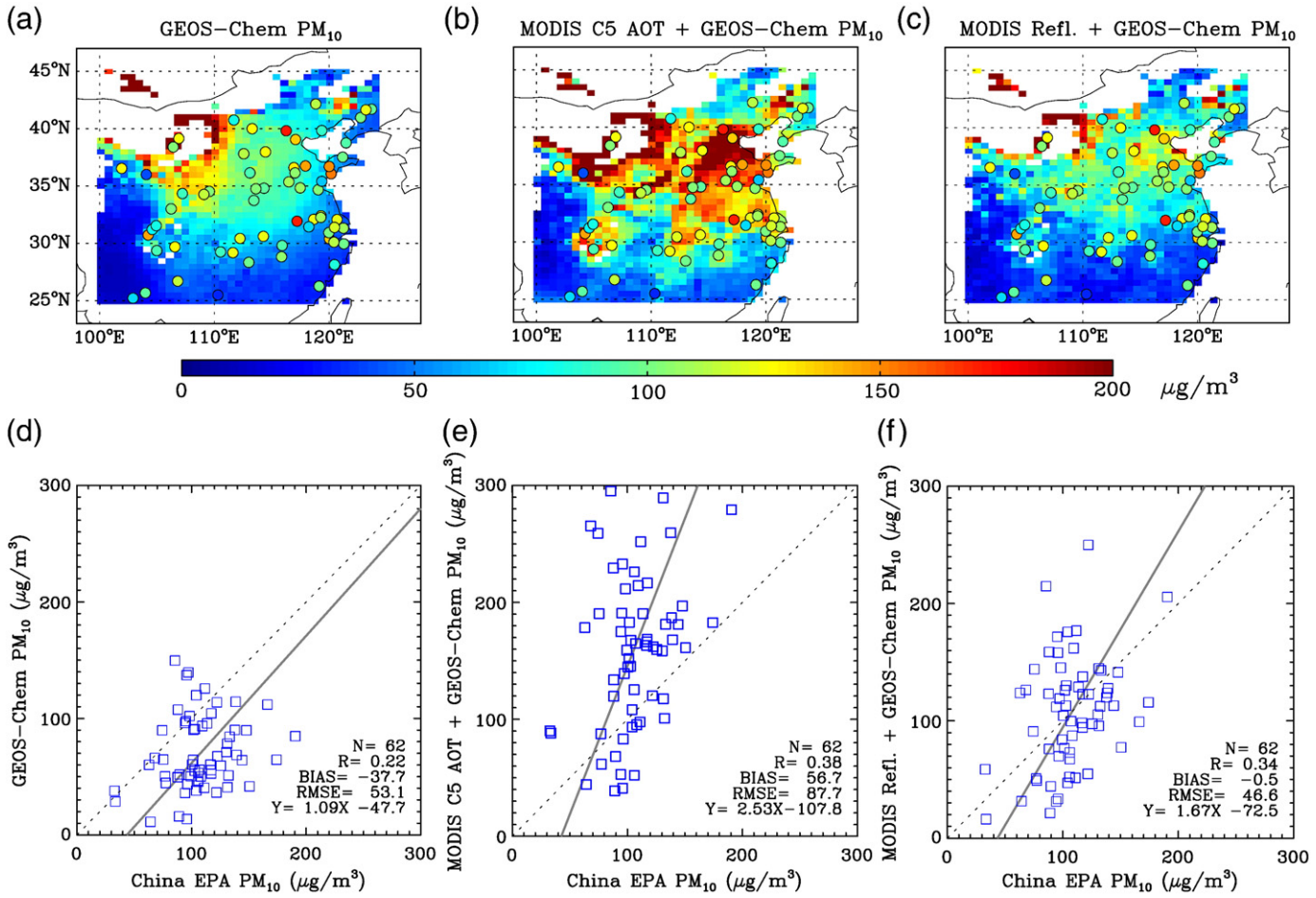

Fig. 4. Distribution of averages of surface PM_{10} mass concentration in April–May 2008, estimated respectively from (a) GEOS-Chem simulation, (b) GEOS-Chem simulation constrained by the MODIS Collection 5 AOT product, and (c) GEOS-Chem simulation constrained by MODIS reflectance (this work). Circles denote locations of 62 Chinese EPA stations, and are color-coded based upon their corresponding averages of measured PM_{10} mass concentration in April–May 2008. (d), (e), and (f) are respectively similar as (a), (b), and (c) but show the scatter plot of the 2-month averages of measured and estimated PM_{10} mass concentration at the 62 cities. Also shown in (d)–(f) are comparison statistics for a total number of data comparison pairs (N): mean bias, root mean square error (RMSE), correlation coefficient (R), and the slope and intercept of the linear regression line (in solid black). The one-to-one fit line is shown in dotted black.

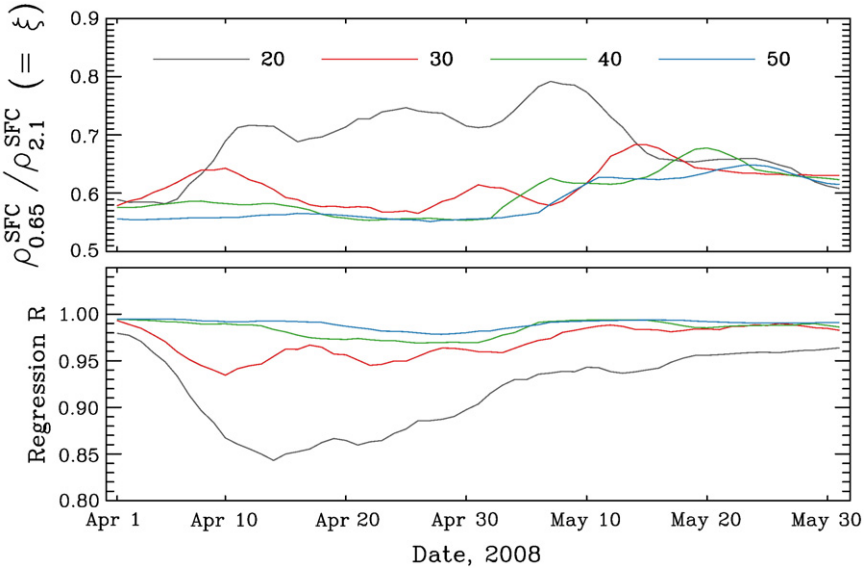

Fig. 5. Top panel: derived surface reflectance ratio (ξ) between the 0.65 μm and 2.1 μm at the AERONET station Xionglong during April 1–May 31, 2008; the derivation is conducted by using "dynamical lower envelope" approach in which the regression is made based upon the MODIS data collected in 20 days (black line), 30 days (red line), 40 days (green line), or 50 days (blue line) center on the day for which ξ is derived. Bottom panel: same as the top panel but shows the regression coefficient R. See the text in Section 3 and the caption for Fig. 2(a) for details.

In Fig. 5, we give one example showing the variation of ξ with different L during April 1–May 31, 2008 over the Xionglong AERONET station. It is clear that the regression for deriving ξ becomes more statistically robust (values of linear regression coefficient R increases) as L changes from 20 to 50 days. However, when L is 40 days or larger, the R values are all greater than 0.95. On any particular day, the changes of R and ξ are both small (<± 3%) as L increases from 40 days to 50 days, thus indicating that 40 days is an optimal duration for using the lower envelope approach to derive ξ. Knapp et al. (2005) applied the composite clear reflectance technique (that also searches to find low-aerosol conditions) to the geostationary satellite data to estimate the surface reflectance, and they found the optimal time period for their technique is 20 days for both spring and summer. Given that the MODIS sensor is installed on polar-orbiting satellites with revisit frequency only once per day at most, our time period of 40 days appears consistent with that used by Knapp et al. (2005).

Another issue that may affect our retrieval and deserves discussion is the assumption of spherical dust particles and Lorenz–Mie scattering calculations of phase functions. Previous studies have shown that non-spherical dust particles have very different phase functions at various backscattering angles when compared to those for spherical particles (Mishchenko et al., 1995). Further investigation of the effect of particle shape on our retrieval accuracy is needed; this will be a major focus in our next study because of the following reasons:

(a) For regions downwind of dust sources (such as over Eastern China in the dusty season), the phase functions of spherical and non-spherical particles are both important for the accurate retrieval of AOT (Wang et al., 2003a,b). Unfortunately, MODIS lacks the multi-angle observations that MISR possesses in order to separate AOT contributions from spherical particle extinction as opposed to non-spherical particle extinction (Kalashnikova et al., 2005).

(b) While GEOS-Chem offers information on the relative mass abundance of dust and fine-mode particles, challenges remain in characterizing the spatio-temporal variability of the particle shape with respect to the particle size of non-spherical particles. Admittedly, the phase function of spheroids or other symmetric convex particles can be computed with

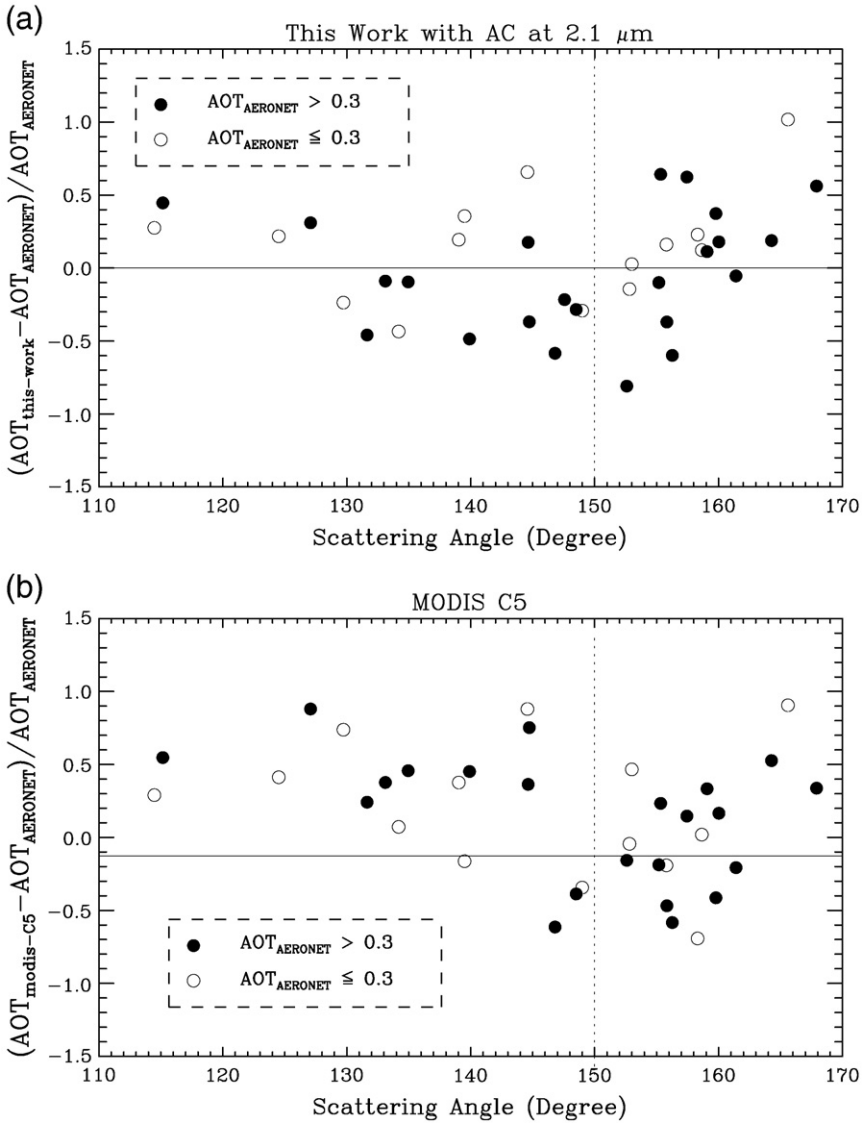

Fig. 6. (a) Relative retrieval error of aerosol optical thickness at 0.65 μm in this work ($AOT_{this-work}$) with respect to the AOT measured from AEROENT ($AOT_{AEROENT}$) as a function of scattering angles. (b) same as (a) but for retrieval error of AOT from MODIS C5 ($AOT_{modis-C5}$). Solid and open circles represent the data points with $AOT_{AEROENT}$ larger and smaller than 0.3, respectively.

existing techniques (such as T-matrix, (Mishchenko and Travis, 1998)) for high accuracy and used in the satellite retrieval algorithm. However, not all dust particles are spheroidal; the phase function differences for spherical particles and concave aggregated non-spherical particles is an active area for research (Mishchenko et al., 2000).

(c) We show in Fig. 6a that our AOT retrievals in either weak ($\tau_{0.67}^{AERT}<0.3$) or strong dusty conditions have no systematic bias with respect to the scattering angle especially at 150° where a transition from positive to negative bias would be expected if dust particles are oblate spheriods but the retrieval uses the spherical particle phase function (Wang et al., 2003a,b). Indeed, the MODIS C5 AOT retrievals show a similar retrieval error pattern with the scattering angle to our AOT retrievals, except the former have a clear positive bias (Fig. 6b). We argue that the lack of a distinct effect due to dust non-spherical particle phase functions on our retrieval (as shown in Fig. 6) appears consistent with the findings by Li and Osada (2007), who showed that only spherical dust particles are persistent downwind of desert regions, because of the preferential settling of elongated dust particles.

5. Summary

This study reinforces previous studies by Weaver et al. (2007) and Drury et al. (2008) on the use the satellite reflectances to constrain CTM simulation of aerosols, and benefits from the use of cloud-screened reflectance over dark pixels saved in the MODIS C5 aerosol product (Levy et al., 2007). However, our algorithm differs from previous approaches in the following aspects: (1) the use of a "dynamic lower envelope" regression to derive locally the surface visible/NIR reflectance ratios on a daily basis, (2) the removal of atmospheric dust effects when applying the NIR reflectance at the top-of-atmosphere to derive surface reflectance, and (3) the use of the Jacobian of reflectance with respect to aerosol optical thickness to update the retrieved AOT and to fasten the convergence between the modeled and MODIS measured reflectance. Because our dynamical lower envelope approach for deriving surface visible/near infrared reflectance ratio uses the MODIS data over a 40-day period centered on the day of the retrieval, our algorithm is not suitable for operational purposes. However, the promising results shown in this study certainly make the approach an attractive option for re-analysis of AOT and surface aerosol concentration, particularly at a regional scale.

Key assumptions in our approach of retrieving aerosol optical thickness and surface aerosol concentration are: (1) GEOS-Chem simulated vertical shape of mass mixing ratio of different aerosol component are kept constant in the retrieval; (2) a generic database of the single scattering properties of each aerosol component (Koepke et al., 1997) with update from Drury et al. (2010) is used in the retrieval; (3) the shape of surface bidirectional reflectance in the visible and near infrared are assumed to be the similar and so that the relationship between visible and near infrared surface reflectance is linear; this assumption has been used in various aerosol retrieval algorithms including those designed for MODIS (Levy et al., 2007; Lyapustin and Wang, 2009) and MISR (Diner et al., 2005), although the methods used in these studies for deriving the ratio between surface visible and near infrared reflectance are different from our "dynamical lower envelope" approach. Hence, the challenges for next steps include the retrieval of aerosol size and aerosol composition from the multi-spectral multi-angle satellite data, as well as the improved estimate of surface reflectance. However, the large RMSEs in all three estimates of PM_{10} (using model only, model with MODIS C5 AOT, and model with MODIS reflectance) shown in Fig. 4d–f certainly highlights the critical need of constraint for aerosol profile, at least for the GEOS-Chem modeling in the region of this study.

Acknowledgments

This research is supported by the NASA Earth Sciences New Investigator Program and Radiation Science Program. We thank the data services provided by the Goddard Earth Science Data Center and the AERONET team in NASA GSFC., and the computational support provided by the Holland Computing Center of the University of Nebraska. J. Wang is grateful to Ralph Kahn for his constructive comments on the early version of this manuscript.

References

Al-Saadi, J., Szykman, J., Pierce, R. B., Kittaka, C., Neil, D., Chu, D. A., et al. (2005). Improving national air quality forecasts with satellite aerosol observations. *Bulletin of the American Meteorological Society*, *86*, 1249−1261.

Anderson, T. L., Charlson, R. J., Winker, D. M., Ogren, J. A., & Holmen, K. (2003). Mesoscale variations of tropospheric aerosols. *Journal of Atmospheric Sciences*, *60*, 119−136.

Chen, D., Wang, Y. X., McElroy, M. B., He, K., Yantosca, R. M., & Le Sager, P. (2009). Regional CO pollution in China simulated by the high-resolution nested-grid GEOS-Chem model. *Atmospheric Chemistry and Physics*, *9*, 3825−3839.

Diner, D. J., Martonchik, J. V., Kahn, R. A., Pinty, B. G. N., Nelson, D. L., & Holben, B. N. (2005). Using angular and spectral shape similarity constraints to improve MISR aerosol and surface retrievals over land. *Remote Sensing of Environment*, *94*, 155−171.

Drury, E., Jacob, D. J., Wang, J., Spurr, R. J. D., & Chance, K. (2008). Improved algorithm for MODIS satellite retrievals of aerosol optical depths over land. *Journal of Geophysical Research*, *113*, D16204. doi:10.1029/2007JD009573

Drury, E., Jacob, D. J., Spurr, R., Wang, J., Shinozuka, Y., Anderson, B., Clark, A., Dibb, J., McNaughton, C., & Weber, R. (2010). Synthesis of Satellite (MODIS), aircraft (ICARTT), and surface (IMPROVE, EPA-AQS, AERONET) aerosol observations over eastern North America to improve MODIS aerosol retrievals and constrain surface aerosol concentrations and sources. *Journal of Geophysical Research*, *115*, D14204.

Fairlie, T. D., Jacob, D. J., & Park, R. J. (2007). The impact of transpacific transport of mineral dust in the United States. *Atmospheric Environment*, 1251−1266.

Hoff, R., & Christopher, S. A. (2009). Remote sensing of particulate matter air pollution from space: Have we reached the promised land? *Journal of the Air and Waste Management Association*, *59*, 642−675.

Holben, B. N., Eck, T. F., Slutsker, I., Tanré, D., Buis, J. P., Setzer, A., Vermote, E., Reagan, J. A., Kaufman, Y. J., Nakajima, T., Lavenu, F., Jankowiak, I., & Smirnov, A. (1998). AERONET- A federated instrument network and data archive for aerosol characterization. *Remote Sensing of Environment*, *66*, 1−16.

Ichoku, C., Chu, D. A., Mattoo, S., Kaufman, Y. J., Remer, L. A., Tanre, D., et al. (2002). A spatio-temporal approach for global validation and analysis of MODIS aerosol products. *Geophysical Research Letters*, *29*(12). doi:10.1029/2002GL013206

Kahn, R. A., Chen, Y., Nelson, D. L., Leung, F. -Y., Li, Q., Diner, D. J., et al. (2008). Wildfire smoke injection heights: Two perspective from space. *Geophysical Research Letters*, *35*, L04809. doi:10.1029/02007GL032165

Kahn, R., Gaitley, B. J., Martonchik, J. V., Diner, D. J., Crean, K. A., & Holben, B. (2005). MISR global aerosol optical depth validation based on two years of coincident AERONET observations. *Journal of Geophysical Research*, *110*, D10S04. doi:10.1029/2004JD004706

Kalashnikova, O. V., Kahn, R., Sokolik, I. N., & Li, W. -H. (2005). The ability of multi-angle remote sensing observations to identify and distinguish mineral dust types: Part 1. Optical models and retrievals of optically thick plumes. *Journal of Geophysical Research*, *110*, D18S14. doi:10.1029/2004JD004550

Kaufman, Y. J., Gobron, N., Pinty, B., Widlowski, J. -L., & Verstraete, M. M. (2002). Relationship between surface reflectance in the visible and mid-IR used in MODIS aerosol algorithm-theory. *Geophysical Research Letters*, *29*. doi:10.1029/2001GL014492

Knapp, K. R., Frouin, R., Kondragunta, S., & Prados, A. (2005). Toward aerosol optical depth retrievals over land from GOES visible radiances: Determining surface reflectance. *International Journal of Remote Sensing*, *26*, 4097−4116.

Koepke, P., Hess, M., Schult, I., & Shettle, E. P. (1997). *Global Aerosol Data Set, Rep. No. 243, Max-Planck-Institut fur Meteorol., Hamburg, Germany*.

Liu, Y., Koutrakis, P., Kahn, R., Turquey, S., & Yantosca, R. M. (2007). Estimating fine particulate matter component concentrations and size distributions using satellite-retrieved fractional aerosol optical depth: Part 2 — A case study. *Journal of the Air and Waste Management Association*, *57*, 1360−1369.

Levy, R. C., Remer, L. A., Mattoo, S., Vermote, E. F., & Kaufman, Y. J. (2007). Second-generation operational algorithm: Retrieval of aerosol properties over land from inversion of Moderate Resolution Imaging Spectroradiometer spectral reflectance. *Journal of Geophysical Research*, *112*, D13211. doi:10.1029/12006JD007811

Lyapustin, A., & Wang, Y. (2009). The time series technique for aerosol retrievals over land from MODIS. In A. Kokhanovky, & G. De Leeuw (Eds.), *Satellite aerosol remote sensing over land* (pp. 69−99). Springer Praxis Books. 978-3-540-69396-3.

Mishchenko, M., Lacis, A. A., Carlson, B. E., & Travis, L. D. (1995). Nonsphericity of dust-like troposheric aerosols: implications for aerosol remote sensing and climate modeling. *Geophysical Research Letters*, *1995*, 1077−1080.

Mishchenko, M., & Travis, L. D. (1998). Capabilities and limitations of a current fortran implementation of the T-matrix method for randomly oriented, rotationally sysmmetric scatters. *Journal of Quantitative Spectroscopy and Radiative Transfer*, *60*, 309−324.

Mishchenko, M. I., Hovenier, J. W., & Travis, L. D. (Eds.). (2000). *Light scattering by nonspherical particles: Theory, measurements, and applications*. San Diego: Academic Press.

Li, L., & Osada, K. (2007). Preferential settling of elongated mineral dust particles in the atmosphere. *Geophysical Research Letters*, *34*, L17807. doi:10.1029/2007GL030262

Park, R. J., Jacob, D. J., Field, B. D., Yantosca, R. M., & Chin, M. (2004). Natural and transboundary pollution influences on sulfate–nitrate–ammonium aerosols in the United States: Implications for policy. *Journal of Geophysical Research*, *109*, 4355. doi:10.1029/2003JD004473

Remer, L. A., Kleidman, R. G., Levy, R. C., Kaufman, Y. J., Tanre, D., Mattoo, S., et al. (2008). Global aerosol climatology from the MODIS satellite sensors. *Journal of Geophysical Research*, *113*, D14S07. doi:10.1029/2007JD009661

Spurr, R. (2008). In A. Kokhanovsky (Ed.), *LIDORT and VLIDORT: Linearized pseudo-spherical scalar and vector discrete ordinate radiative transfer models for use in remote sensing retrieval problems. Light Scattering Reviews*, *vol. 3*, Springer.

Torres, O., Tanskanen, A., Veihelmann, B., Ahn, C., Braak, R., Bhartia, P. K., et al. (2007). Aerosols and surface UV products from Ozone Monitoring Instrument observations: An overview. *Journal of Geophysical Research*, *112*, D24S47. doi:10.1029/2007JD008809

Wang, J., & Christopher, S. A. (2003). Intercomparison between satellite-derived aerosol optical thickness and PM2.5 mass: Implications for air quality studies. *Geophysical Research Letters*, *30*, 2095. doi:10.1029/2003GL018174

Wang, J., Christopher, S. A., Reid, J. S., Maring, H., Savoie, D., Holben, B. H., et al. (2003a). GOES 8 retrieval of dust aerosol optical thickness over the Atlantic Ocean during PRIDE. *Journal of Geophysical Research*, *108*, 8595. doi:10.1029/2002JD002494

Wang, J., Hoffmann, A. A., Park, R., Jacob, D. J., & Martin, S. T. (2008). Global distribution of solid and aqueous sulfate aerosols: Effect of the hysteresis of particle phase transitions. *Journal of Geophysical Research*, *113*, D11206. doi:10.1029/2007JD009367

Wang, J., Liu, X., Christopher, S. A., Reid, J. S., Reid, E. A., & Maring, H. (2003b). The effects of non-sphericity on geostationary satellite retrievals of dust aerosols. *Geophysical Research Letters*, *30*, 2293. doi:10.1029/2003GL018697

Wang, J., Nair, U., & Christopher, S. A. (2004). GOES-8 aerosol optical thickness assimilation in a mesoscale model: Online integration of aerosol radiative effects. *Journal of Geophysical Research*, *109*, D23203. doi:10.1029/2004JD004827

Weaver, C., Silva, A. D., Chin, M., Ginoux, P., Dubovik, O., Flittner, D., et al. (2007). Direct insertion of MODIS radiances in a global aerosol transport model. *Journal of Atmospheric Sciences*, *64*, 808−826.

van Donkelaar, A., Martin, R. V., Brauer, M., Kahn, R., Levy, R., Verduzco, C., & Villeneuve, P. J. (2010). Global estimates of ambient fine particulate matter concentrations from satellite-based aerosol optical depth: Development and application. *Environmental Health Perspectives*, *118*, 847−855. doi:10.1289/ehp.0901623